Journal of
Applied Crystallography
ISSN 0021-8898

Received 30 July 1999
Accepted 2 December 1999

Next-near-neighbour interactions with Al in Li^+- and Rb^+-exchanged Na^+ β-aluminas, detected by synchrotron X-ray absorption spectroscopy

Augusto Marcelli,[a]* Annibale Mottana[b] and Giannantonio Cibin[a]

[a]Istituto Nazionale di Fisica Nucleare, Laboratori Nazionali di Frascati, Via E. Fermi 40, I-00044 Frascati RM, Italy, and [b]Universita' degli Studi Roma Tre, Dipartimento di Scienze Geologiche, Largo S. Leonardo Murialdo 1, I-00146 Roma RM, Italy. Correspondence e-mail: augusto.marcelli@lnf.infn.it

Synchrotron X-ray absorption near-edge structure (XANES) spectroscopy studies have been carried out on the electronic and crystal structure environments around the Al atom in Na^+ β-alumina and in two β-aluminas with Na^+ exchanged by Li^+ and Rb^+. The aim is to define the type of interaction, if any, existing between the Al located in the 'spinel block' and the fast-conducting cations in the 'conduction plane'. Na^+ β''-alumina has also been studied for comparison. All β-alumina spectra differ from that of α-alumina (corundum) by showing additional features due to the presence of tetrahedral Al. Moreover, they all show a much greater degree of local disorder. There are definite, but small, interactions between tetrahedral Al (and, possibly, also octahedral Al) in the 'spinel block' and the Na^+ and Rb^+ cations in the 'conduction plane'; Na^+ and Rb^+ β-aluminas have similar Al *K*-edge XANES features, but with intensities that change in relation to the weight of the 'conduction plane' atom. Despite differences in composition and structure, Na^+ β''-alumina shows the same behaviour, thus confirming the substantial similarity of the Al local environments. Li^+-exchanged β-alumina has an Al *K*-edge XANES spectrum that apparently differs from all others, but actually conveys the same basic information. Indeed, interaction between Al and Li is much greater than in any other β-alumina because Li^+ moves laterally off the 'conduction plane' to become close to a facing tetrahedral Al, and strongly interacts with it. Thus, this study also draws attention to the fact that β-aluminas react differently to alkali exchange.

1. Introduction

Sodium β-alumina is the prototype of a family of artificial ionic fast conductors showing powerful two-dimensional transport properties even at moderate temperatures (*e.g.*, Kummer & Weber, 1968; Roth *et al.*, 1976; Collin *et al.*, 1980) as well as other interesting properties (*e.g.*, Tietz & Urland, 1992). This behaviour arises from the unusual crystal structures which, although they may be classified in various subfamilies (*i.e.*, the β-, β'- and β''-aluminas), are similar enough across all phases so as to make them equally suitable for industrial applications.

The essential features of the Na^+ β-alumina crystal structure were originally determined (Bragg *et al.*, 1931) under the assumption that the compound was essentially pure Al_2O_3, as stated in the first synthesis carried out on a poorly controlled starting composition (Rankin & Merwin, 1916). The non-stoichiometric Na^+ ions found to be present in excess were randomly distributed over the entire structure; however, the resulting composition turned out to be inconsistent with the determined space group and site occupancies. A re-determination (Beevers & Ross, 1937) made under the assumption that the chemical formula was $Na_2O.11Al_2O_3$ resulted in the following findings: (i) Na^+ β-alumina consists of compact Al_2O_3 blocks having the defect-spinel structure; (ii) these blocks sandwich tiny, loosely packed, diatomic Na–O layers; (iii) all atoms are in fixed ordered positions with full occupancy (Fig. 1). However, refinements became necessary after chemical and synthesis work had demonstrated that (*a*) Na atoms are usually present in excess of the 1:11 Na:Al ratio and may vary over a large range (to 1:8.1$\sim$1:9.2; Yao & Kummer, 1967; Weber & Venero, 1969), and (*b*) Na^+ can be exchanged with all alkalis and many other cations (*e.g.*, Yao & Kummer, 1967; Roth, 1972; Le Cars *et al.*, 1974; Roth *et al.*, 1976; Briant & Farrington, 1980; Boilot *et al.*, 1980; Sattar *et al.*, 1986). Furthermore, the disclosure that nearly all the exchanged cations showed very high mobility (Kummer & Weber, 1968; Briant & Farrington, 1981; *cf.* Alfrey *et al.*, 1988) fostered a

series of increasingly accurate structural studies by means of a variety of methods. New refinements were made using X-ray (Felsche, 1967; Kato, 1968; Bettman & Peters, 1969; Peters *et al.*, 1971; Roth, 1972; Boilot *et al.*, 1980; Jorgensen *et al.*, 1981; Dudney *et al.*, 1981; Bates *et al.*, 1982; Collin, Boilot *et al.*, 1986*a*,*b*; Carrillo-Cabrera *et al.*, 1988; Dunn, Schwarz *et al.*, 1988; Dunn *et al.*, 1989; Edström, Thomas *et al.*, 1991*a*,*b*,*c*; Bera, 1992; Wolf & Thomas, 1993; Edström *et al.*, 1997) and neutron diffraction (Reidinger, 1979; Tofield & Farrington, 1979; Bates *et al.*, 1982; Edström *et al.*, 1997). Moreover, all possible experimental techniques were applied to the purpose of elucidating the individual characteristics of each compound and the general properties of the family; these techniques include transmission electron microscopy (Cheng *et al.*, 1994), optical absorption (Alfrey *et al.*, 1988; Dai & Stafsudd, 1991), X-ray scattering (Boilot *et al.*, 1980; Collin, Boilot *et al.*, 1986*a*), Raman scattering (Kaneda *et al.*, 1978; Bates *et al.*, 1982; Mariotto *et al.*, 1985), electron paramagnetic resonance (Dunn, Yang & Vivien, 1988) and X-ray absorption spectroscopy (Wong, Roth *et al.*, 1986; Bush *et al.*, 1992; Den Boer *et al.*, 1992; Rocca *et al.*, 1994*a*,*b*, 1996; Wilkinson, 1997). Furthermore, theoretical methods of prediction and evaluation, such as molecular dynamics, have been used (Catti *et al.*, 1987; Zendejas & Thomas, 1990; Edvardsson *et al.*, 1992). Together, these studies have shown the following (see also Figs. 1 and 2).

(*a*) The basic structure consists of parallel Al_2O_3 slabs made up of several layers (four in β-alumina, strictly) of O anions in a nearly ideal cubic closest packing arrangement, lying on the *ab* plane with the metal in the interstices arranged according to the defect-spinel structure. This is the structure of the $MgAl_2O_4$ type, in which the 16 octahedral voids and 8 tetrahedral voids among the 32 O anions are occupied by Al^{3+} cations only, although in a reduced number to approach electrostatic neutrality ($\sim$21 out of 24 cation sites, *i.e.* $\sim$14 Al^{3+} in eightfold coordination and $\sim$7 Al^{3+} in fourfold coordination). This portion of the unit cell is the 'spinel block', the residual electrostatic imbalance of which is made up by inter-block cations, typically Na^+.

(*b*) Adjacent 'spinel blocks' are related to each other by *ab* mirror planes at z = 1/4 and 3/4, and linked together in the *c* direction by the O(5) oxygens of Al(3)—O(5)—Al(3) bonds, running vertically across the inter-block layer. The mirror planes coincide with the 'conduction planes', *i.e.* these mirror planes contain the fast-moving Na^+, *viz* exchanged cations that are required in order to attain charge balance. The bridging O(5) oxygens that lie on these planes ('column oxygens') form a hexagonal lattice.

(*c*) The fast-moving cations on the 'conduction plane' may be located in no less than four sites (Fig. 2): (i) Beevers–Ross (BR) sites, *i.e.* those originally detected at 2/3 1/3 1/4 by Beevers & Ross (1937) when solving the β-alumina structure as ordered and with full Na occupancy; (ii) anti Beevers–Ross (aBR) sites, at 0 0 1/4, first defined by Peters *et al.* (1971) with the aim of accommodating Na in excess over the theoretical $Na_2O.11Al_2O_3$ composition, but actually found to be empty in Na^+ β-alumina, and occupied in Ag^+ β-alumina (Roth, 1972);

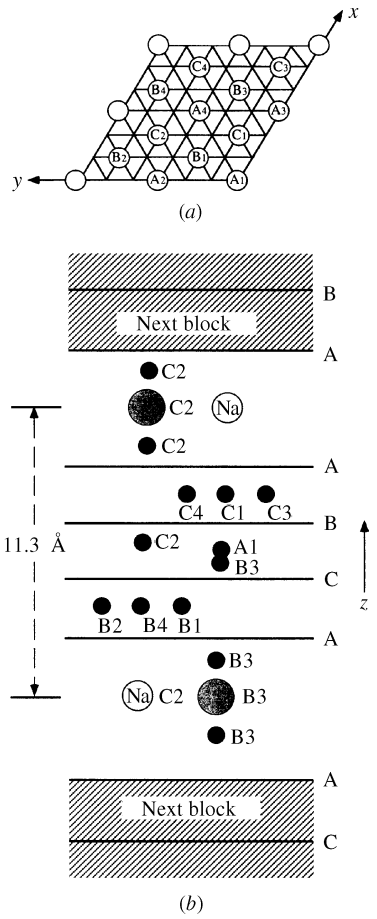

Figure 1
The structure of Na^+ β-alumina as originally determined by Beevers & Ross (1937) assuming a composition of $Na_2O.11Al_2O_3$ [after Peters *et al.* (1971) Fig. 1, slightly modified]. (*a*) *ab* section of the unit cell showing the A, B and C positions of the cations. (*b*) Schematic *bc* projection, with A, B and C indicating the close-packed oxygen layers in which all A, or B, or C positions are occupied; black dots are Al cations in the x–y positions labelled in (*a*); the Na and O ions in the conduction layer are circled and labelled according to their position in the *ab* plane.

(iii) the mid-oxygen (mO) site, at or near 5/6 1/6 1/4, defined again by Peters *et al.* (1971) for the same purpose (and actually occupied in the Na^+-bearing specimen they had refined); and (iv) a non-precisely located, interstitial site (A) that Edström, Thomas *et al.* (1991*a*) refined to host some additional Na^+. Finally, to increase variability further, one should remember also (v) the Roth–Reidinger (RR) site, which is a Frenkel defect, first dected by Roth *et al.* (1976), where extra Na^+ plus compensating O(6) anions on the 'conduction plane' are stabilized by interstitial Al(5) displaced from the normal Al(1) site in the 'spinel block'. This Frenkel defect has negative effects on ion mobility in that it blocks some of the possible pathways of the 'conduction plane'.

(*d*) All sites need not be fully occupied at the same time, and the cations on the 'conduction plane' are actually loosely bound, so that in many cases their positional parameters are not fractional but irrational, and must be determined case by case. Irrational atomic coordinates have been refined also for some of the Al ions located in the 'spinel block'; they were

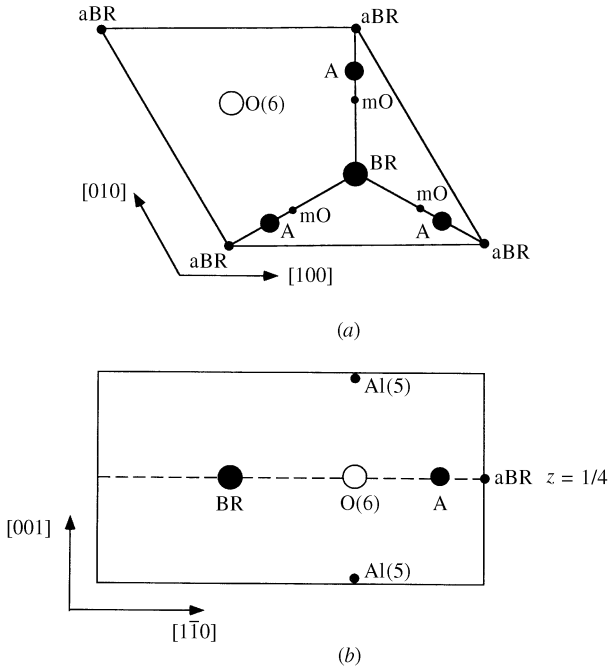

Figure 2
The structure of Na^+ β-alumina after Edström, Thomas *et al.* (1991*a*; Fig. 1, slightly modified). (*a*) Projection of the 'conduction plane' on *ab* with all possible positions where the fast-conducting Na^+ cation may go (BR, aBR, mO and A sites) and two of the positions taken by the O anions: O(5), the 'column oxygen' lying in the 'conduction plane' and connecting the 'spinel blocks', and O(6), at z = 1/4, *i.e.* above and below. (*b*) Projection on the vertical plane across the 'conduction plane', showing the locations of the Na cations and of tetrahedral Al(5) cations of the 'spinel blocks' above and below, both these being bound to the O(6) on the 'conduction plane' to form the 'column'.

interpreted as resulting from adaptation of the whole atomic structure to the electrical instability locally induced by the ionic fast conductors moving in the nearby 'conduction planes'.

(*e*) Despite these local defects, all β-aluminas (strictly speaking) possess hexagonal symmetry, whereas β''-aluminas are trigonal with their 'spinel block' containing three layers. These compounds [first synthesised by Thery & Briançon (1962)] trend back towards the spinel true formula, as they contain divalent cations (usually Mg, rarely Fe) replacing Al^{3+} in the tetrahedral Al(2) position of the 'spinel block'; to balance this, they incorporate *via* cation exchange either alkali ions in excess or even significant amounts of trivalent transition and rare-earth metal atoms. These cations are located in the 'conduction plane' (which is no longer a mirror) and are mobile in that they distribute disorderly over the BR and aBR (no longer independent) sites, and the mO sites. The concomitant effect of the trivalent and divalent new cations on the overall structure may be so large as to even significantly dislodge the O anions and Al cations from their expected sites in the 'spinel block'.

(*f*) Despite the structural difference, all β-aluminas belong to the same chemical family, the general formula of which is $(Al_{11-y}Mg_yO_{16})[Alk_{1+x+y}O_{1+x/2}]$, where the curved parentheses include the ions located in the 'spinel block' (the number of layers of which determines the symmetry of the overall structure) and the square brackets contain the mobile ions in the 'conduction plane'; the two parts are related *via* a double compensation mechanism (Collin *et al.*, 1988).

Most previous studies concerned the fast-conducting cations of the 'inter-block layer' in view of the potential industrial applications they give to the compounds. Here, we will focus on the local environment and electronic properties of Al, the main atom, located in the 'spinel block' only.

Our aim is to detect the extent of Al involvement in the structural and electrostatic changes induced by the presence in the inter-block layer of different fast-conducting cations. Thus we hope to contribute to a better understanding of the local electronic properties of Al in the β-alumina family, as we did previously for other synthetic α-alumina compounds, also useful for their industrial properties (Mottana *et al.*, 1998).

2. Experimental

2.1. Samples

Platy ~4 × 2 mm single-crystal blades, ~0.05 mm thick, of β-aluminas were provided by G. Mariotto (University of Trento; *cf.* Rocca *et al.*, 1994*a*,*b*, 1996). These were a 100% pure Na^+ β-alumina grown by flux evaporation by Union Carbide, the nominally 100% Li^+ and Rb^+ derivatives obtained from it by cation exchange in molten chlorides (by G. Mariotto), and a 100% pure Na^+ β''-alumina, also grown by flux evaporation, by G. C. Farrington, Philadelphia, USA. Pure α-Al_2O_3 and $MgAl_2O_4$ were provided as powders by Bayerisches Geoinstitut, Bayreuth, Germany, courtesy of F. Seifert.

2.2. X-ray absorption near-edge structure (XANES) spectroscopy

High-resolution X-ray absorption spectroscopy measurements were carried out at the Stanford Synchrotron Radiation Laboratory (SSRL), where SPEAR, the electron storage ring, operated at 3.0 GeV with the circulatory current decreasing from ~90 to ~60 mA during a time span of 12~16 h. The Al *K* edges were recorded at beamline SBO3-3 under high vacuum (10^{-7} torr), using the JUMBO monochromator of the double-crystal type (Hussain *et al.*, 1982) consisting of two plates from the same YB_{66} crystal cut along the 400 plane (Wong *et al.*, 1990). The spectral acquisition range was from 1540 to 1690 eV, counting at 0.3~0.5 eV intervals for 2~4 s at a time. We operated in the 'total electron yield' (TEY) mode (Erbil *et al.*, 1988). Experimental resolution was certainly better than 0.55 eV (Schaefers *et al.*, 1992) and estimated to be 0.46 eV (Michael Rowen, personal communication). Specimens were made to adhere on the flat silvered sample holder and fastened with kapton tape. Metallic Al foil was used as a reference for energy calibration, and in addition pure synthetic α-Al_2O_3 powder (Mottana *et al.*, 1998; Fig. 1) served as a secondary standard. Great care was taken of the absorption-edge energy drift during data acquisition. It was corrected by recording at regular time intervals the secondary

standard and by calibrating its main-edge energy value against the ring current. As an additional calibration, we checked the alignment of all spectra using a glitch at 1594 eV, intrinsically occurring in the YB_{66} crystal (Wong *et al.*, 1994). The measured spectra were 'background subtracted' using the careful mathematical methods that are normally used in dichroism experiments, where the weak signals to be detected are in the range 10^{-3}∼10^{-4} times the absorption signals (Chaboy *et al.*, 1998; see also Mottana *et al.*, 1998). The energy values of all features were then measured by fitting Lorentzian lines, and normalized to 1.0 at high energy, *i.e.* 1605 eV (Bianconi, 1988). Overall, the data have errors (at the 2σ level) always below 0.1 eV for energy and 5% for relative intensity.

3. Experimental results

The normalized experimental Al *K*-edge spectra are reported in full in Fig. 3 and, in greater detail, in Fig. 4. Throughout, the data are compared with those of synthetic α-alumina, our secondary standard and reference compound (Mottana *et al.*, 1998), and of synthetic $MgAl_2O_4$ spinel.

β-Aluminas display a complex Al *K* edge consisting of at least six features in the full multiple-scattering (FMS) region (often called 'edge region') (Natoli & Benfatto, 1986), which in this system extends to 12∼13 eV above the threshold (Fig. 4: 1563∼1576 eV). Two more features at least, both rather weak and broad, follow in the intermediate multiple-scattering (IMS or 'XANES') region, *i.e.* up to 1605 eV, and mark the onset of the large oscillations typical of the single-scattering (SS or 'EXAFS') regime (Fig. 3). Four major features may be detected (*A*, *C*, *D* and *F*) in all samples; by contrast, *B* is properly defined only in Na^+ β-alumina and *E* is a shoulder that is clearly seen in the Li^+ β-alumina spectrum only. Na^+ and Rb^+ β-aluminas have very similar spectra, their small differences being only in the relative intensities of their features. Indeed, on going from Na^+ to Rb^+, the relative intensities of peaks *A* and *B* decrease slightly, while those of *C* and *D* increase (Fig. 5). This indicates a correlation of the Al *K*-edge peak intensities with the atomic number of the

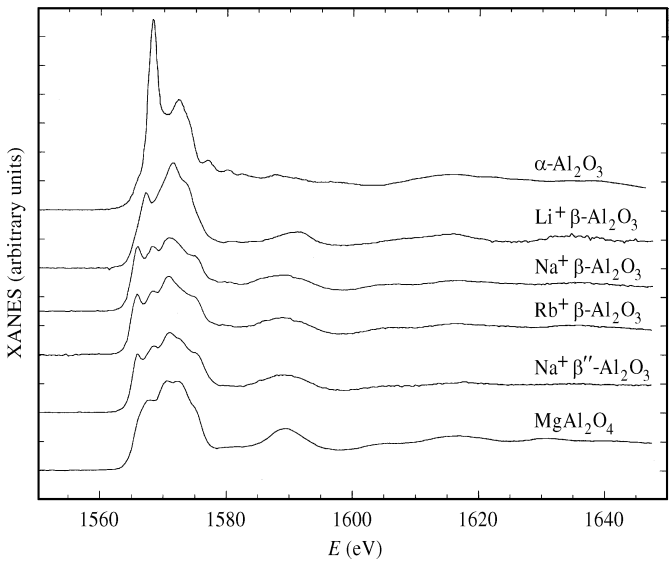

Figure 3
Experimental X-ray absorption spectra at the Al *K* edge for synthetic β- and β''-aluminas and reference α-alumina and $MgAl_2O_4$ spinel.

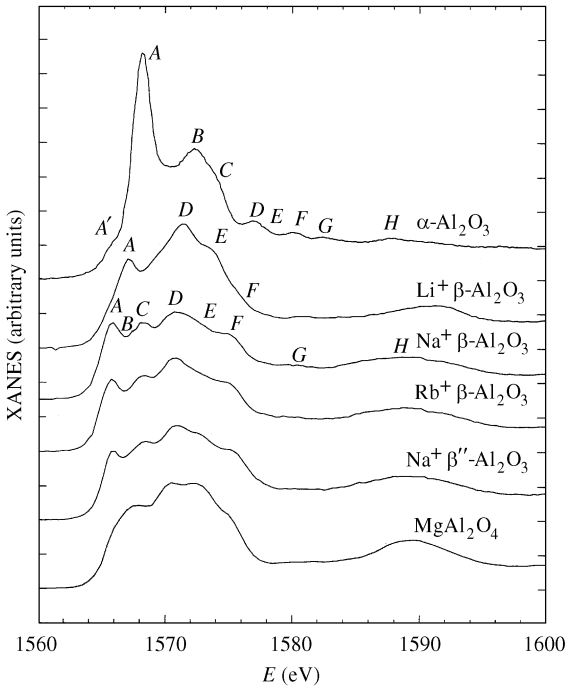

Figure 4
Expanded view in the full multiple-scattering and nearby intermediate multiple-scattering regions of the experimental X-ray absorption spectra of Fig. 3. Peak assignment of α-alumina is the same as that by Mottana *et al.* (1998).

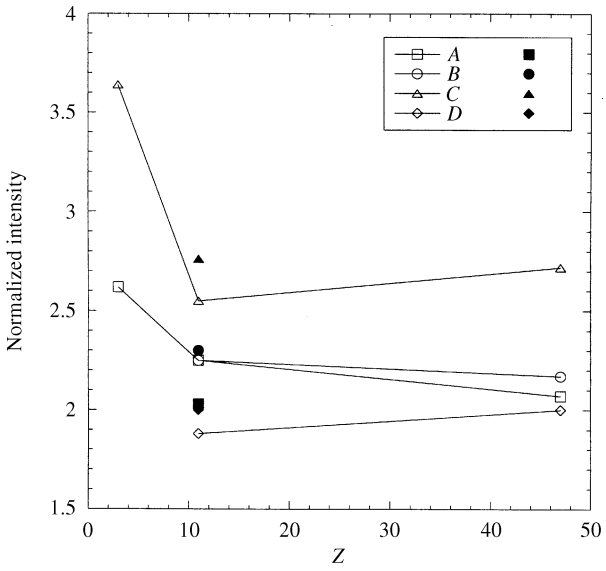

Figure 5
Heights of the major absorption peaks of Li^+, Na^+ and Rb^+ β-aluminas (open symbols and tie-lines) and Na^+ β''-alumina (solid symbols) as a function of the atomic number of the cation located in the 'conduction plane'.

element located in the 'conduction plane'. Therefore, we argue that an electronic interaction between the Al atom that is located inside the 'spinel block' and the next-neighbour cation located outside, in the 'conduction plane', certainly exists, but we consider it to be slight.

Na^+ β''-alumina essentially fits into the same framework (Fig. 4). Its FMS region too displays four major features and, in addition, shoulder *E* is resolved well enough so as to be reliably measurable with respect to both energy (1572.7 eV) and relative intensity (2.5). However, the Na^+ β''-alumina peak intensities do not fit into the β-alumina variation pattern (Fig. 5): feature *A* is too weak while *C* and *D* are too strong with respect to those of Na^+ β-alumina. The difference between the two Na^+-bearing aluminas is better seen when subtracting their normalized spectra (Fig. 6*a*). Although at a first glance the spectra of the two phases almost superimpose, in fact they show differences in the intensities of all their features that reach as much as 5% of the total absorption signal, *i.e.* they far exceed the accuracy of our background-subtracted spectra. The first negative structure in the spectrum, associated with peak *A*, is assigned to a difference in the local and partial densities of states (DOS); thus it may be related to the partial substitution of Mg for Al in the tetrahedral site of β''-alumina. The increased intensity of the remaining FMS region deconvolutes into five positive features, which substantially support the presence of small distortions differentiating the two phases. Therefore, such a complex structure relates to the structural changes occurring in the Al_2O_3 slab, which in a β''-alumina consists of three layers rather than four, and carries with it a decrease in weight of the Al contribution to the spectrum. Very weak but structured differences occur throughout the IMS region too, and suggest the presence of a different order around the Al sites (*cf.* Mottana *et al.*, 1998).

A similar comparison performed by subtracting the Rb^+ and Na^+ β-alumina spectra (Fig. 6*b*) shows less structured differences. At the edge proper there is a very small decrease of the *A* and *B* peak intensities, which corresponds to a small negative difference in DOS, while at higher energies the positive differences resulting from the increase of *C* and *D* are probably related to the change of the cation in the 'conduction plane' (Fig. 5).

Thus, XANES confirms that β- and β''-aluminas belong to the same structural family, although peculiarities are such as to let β''-alumina be set apart in a sub-family of its own. The family would comprise γ-alumina too, at least judging by the spectrum recorded by Doyle *et al.* (1999), but certainly neither α-alumina nor corundums (Mottana *et al.*, 1998), nor Linde alumina, which is a mix of $\alpha + \gamma$ (Doyle *et al.*, 1999).

The Li^+-exchanged β-alumina has an Al *K*-edge spectrum of its own, in spite of the affinities that tie it into the β-family too (Figs. 3 and 4). Indeed, features *A* and *D* in the FMS region are present, although being displaced to higher energy by as much as +1.5 eV; moreover, they are much stronger than the features present in any other β-alumina (Fig. 5). Features *C* and *F* cannot be seen, at least clearly, because *C* might actually be concealed under the rising limb of *D* owing to the overall +1.5 eV energy shift of the edge (Fig. 4). This cannot be the case for feature *F* (see later). Moreover, the Li^+ β-alumina spectrum shows a shoulder *E* at the same energy as that present in Na^+ β''-alumina, but considerably stronger than it. It is quite clear that something occurs in Li^+ β-alumina that strongly modifies the Al interaction properties: this is especially clear when inspecting the intensity variation pattern of Fig. 5.

The IMS regions of all β-aluminas have very few, weak features, the most significant being a broad bump at ~1590 eV (Fig. 3).

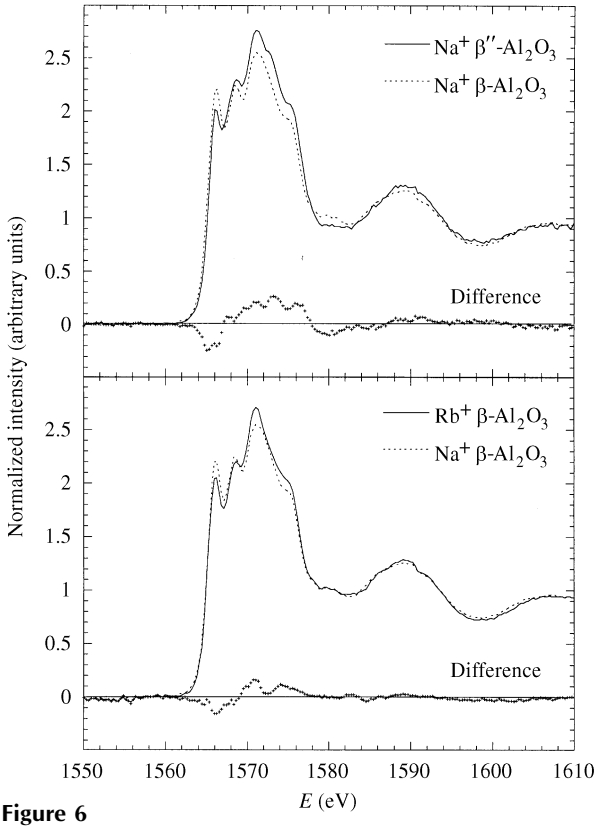

Figure 6
Difference spectra for critical samples. (*a*) Superimposed spectra of Na^+ β''-alumina and Na^+ β-alumina (above) and their difference (below). (*b*) Superimposed spectra of Rb^+ and Na^+ β-alumina (above) and their difference (below).

4. Discussion

Before turning to interpretation, it is worthwhile comparing the β-alumina spectra to that of α-alumina (corundum), which was evaluated and discussed in detail recently in a companion paper to this one (Mottana *et al.*, 1998).

The very first indication arising from inspection of Fig. 3 is that the structures of β-aluminas are significantly more disordered than the α-alumina structure. Indeed, the latter spectrum displays numerous well resolved and sharp features in the IMS region, which have been demonstrated to arise from medium- to long-range order in the $\geq$ 90-atom Al + O cluster surrounding the Al absorber over a sphere of ~0.6 nm in radius (Mottana *et al.*, 1998). The same consideration

applies to the Al *K*-edge spectrum of $MgAl_2O_4$ and confirms the high-ordered structure of this compound, the IMS region of the spectrum of which is indeed sharpest. By contrast, all β-aluminas have poor, weak and broad IMS spectra. Nevertheless, even the broad *H* feature occurring at ~1590 eV in all β-aluminas has its meaning and becomes significant, particularly when one notices that in Li^+ β-alumina it is positively shifted by ~2.3 eV with respect to all other β-aluminas, by ~3.3 eV with respect to α-alumina, and by ~4.2 eV with respect to spinel. Given the substantial overall similarity of all the alumina chemical and structural systems, and taking Natoli's rule for granted, *i.e.* the inverse relationships existing between absorption energy and interatomic distance (Natoli & Benfatto, 1986), these positive shifts imply that: (i) the Al—O bonds of β- and β''-aluminas are on average shorter than those of α-alumina and even more so than those of spinel; in particular, (ii) those of Li^+ β-alumina are shorter than those of all other β- and β''-aluminas, including the actual Na^+ β-alumina from which the Li^+-exchanged sample had been produced by reaction in molten LiCl. Furthermore, if this broad band is indeed the equivalent of feature *H* in α-alumina and spinel (Fig. 4), then the shift observed in the Li^+-bearing β-alumina implies also that a number of multiple-scattering paths are activated, which, besides being significantly shorter, are also differently oriented than those activated in the reference compounds. In other words, XANES independently points out that the entire Al + O structural organization undergoes significant modifications not only when passing from α- to β-alumina (which is obvious, see later), but also when a small cation like Li^+ enters the β-structure *via* Na^+ exchange.

Turning now to the evaluation of the Al *K*-edge spectral features of the β-aluminas, firstly we recall that β-aluminas contain one third of their Al in fourfold coordination, while α-alumina and spinel have all their Al in octahedral coordination. This implies that in the β-aluminas, 1/3 of the Al—O bonds must be shorter than the others; *e.g.* in Na^+ β-alumina the mean bond distances are 0.1731 nm for the smallest tetrahedron, centred by Al(5), and 0.1801 nm for the largest, Al(2), against as much as 0.1893 and 0.1916 nm for two octahedra centred by Al(4) and by Al(1), respectively (Edström, Thomas *et al.*, 1991*a*). As a matter of fact, all polyhedra are very distorted, so that if the Al—O bonds are considered individually, their lengths spread almost continuously over the range 0.1672 ~ 0.2021 nm (Edström, Thomas *et al.*, 1991*a*).

This situation is reflected in the spectra in two ways (Fig. 4): (i) by giving rise to two strong absorption features instead of one, the first of which (*A*) refers to tetrahedral Al and is negatively shifted by ~4 eV with respect to the following one (*C*), which refers to octahedral Al; (ii) by inducing broadening of both these two diagnostic absorption features and all those that follow, which are generated by interaction of the photoelectron emitted by Al with the O atoms located in higher-order coordination shells in the same 'spinel block', as well as with the alkali ions in the 'conduction plane'.

The occurrence of negative energy shifts in the absorption spectra of any atom when its coordination decreases has been known for some time (*e.g.*, for Al: McKeown *et al.*, 1985; *cf.* Wong *et al.*, 1994) and used as a practical tool to establish the coordination of unknown compounds (*e.g.*, Mottana, Robert *et al.*, 1997), although it was found to vary very considerably among different mineral systems (2.2 ~ 5.2 eV; *cf.* Mottana *et al.*, 1998). In simple binary compounds like alumina, its value is essentially independent of structure effects and corresponds to a decrease in the Al—O bond distance only; however, according to Natoli's rule, the 4.0 eV negative shift observed in Na^+ β-alumina would correspond to a shrinkage that is much less than the average bond contraction determined by single-crystal X-ray diffraction refinement (SC-XRef) (0.0165 nm; Edström, Thomas *et al.*, 1991*a*). On the other hand, the aforementioned spectral broadening is intrinsic in the wide spread of Al—O bond lengths measured for the β-aluminas, and affects both the tetrahedra and the octahedra. Such broadening does not occur in α-alumina, in which the octahedron, although deformed to point symmetry 3, has only two sets of precisely defined Al—O bonds [0.1856 and 0.1969 nm (Newnham & deHaan, 1962)], nor in spinel, the AlO_6 octahedron of which is extremely regular with a single set of Al—O bonds, which are 0.1926 nm long (Fischer, 1967).

In α-alumina, our multiple-scattering calculations (Mottana *et al.*, 1998), which were carried out by using dipole approximations only, clearly showed that the very weak first shoulder A' at 1565.8 eV is due to hybridization between the Al *p* orbitals and the empty *p* orbitals of the outer O shells probed by the photoelectrons, provided that a radius of interaction as large as 0.6 nm and a cluster containing more than 90 Al + O atoms is taken into consideration. This interpretation holds true also for β-aluminas, but only to a very minor extent. As a matter of fact, the intensity of the first peak *A* is greatly magnified by the superimposing contributions of two intervening factors: (i) the electronic interaction of Al with the fast-conducting ions of the 'conduction plane', and (ii) the characteristic absorption *K* edge of the fraction of Al present in fourfold coordination (one third of the total Al), which is negatively shifted in comparison with the absorption edge of octahedral Al. Such a peak is not detectable in the spinel spectrum, because all Al is in regular octahedral environments.

Therefore, peaks *A* and *C* in the β-alumina spectra are to be seen as essentially atomic features arising from short-range order, for Al in tetrahedral and octahedral coordination, respectively; as such, their energies are characteristically very constant. All other peaks are features that mark a medium- to long-range structural order, *i.e.* they arise from interactions of the photoelectron emitted by Al with atoms in higher coordination spheres (*cf.* Wu *et al.*, 1996). These atoms are both the O and Al of the 'spinel block', as well as the fast-conducting alkali ions of the 'conduction plane'. Such alkali ions are intrinsically mobile because they are located in many underfilled sites; therefore, it is no wonder that such complex and multiple photoelectron interactions give rise to blurred broad peaks that become very broad indeed in the IMS region.

The comparatively low intensity of feature *A* in Na^+ β''-alumina finds now an easy explanation: according to X-ray diffraction evidence, in this compound the Al(2) site is taken over by Mg^{2+} (Boilot *et al.*, 1980), and only the Al(3) site is available for fourfold-coordinated Al^{3+}, if any. As a matter of fact, the still significant height of the *A* peak in our Na^+ β''-alumina spectrum suggests the presence of significant tetrahedral Al^{3+}, and this might support the inference that some Mg^{2+} cations enter at random the octahedral Al(1) or Al(4) sites, thus leaving more Al^{3+} cations free to enter the Al(3) tetrahedron. SC-XRef reports are either silent on this matter, or claim that they were forced to disregard this detail for technical reasons (Wolf & Thomas, 1993). We recorded an Mg *K*-edge spectrum of Na^+ β''-alumina and found it to be very weak, but with the main feature at 1311.5 eV, *i.e.* just +0.5 eV above that occurring in spinel $MgAl_2O_4$, the Mg of which is well known to be entirely in tetrahedral coordination. Our spectrum gives no indication of octahedral Mg. Consequently, we assume that in our Na^+ β''-alumina, the small fraction of Mg^{2+} is entirely located at the Al(2) site, possibly together with some Al^{3+}, while Al(3) hosts most tetrahedral Al^{3+}, which generates the *A* peak.

The peculiar Li^+ β-alumina Al *K*-edge spectrum deserves a detailed interpretation of its own, not least because Li^+ β-alumina is one of the best solid ionic conductors (Briant & Farrington, 1981), with wide potential industrial applications.

The available structural information is equivocal. According to an early powder neutron diffraction study (Tofield & Farrington, 1979) the Li^+ ions are located by as much as 0.1 nm outside and on either side of the 'conduction plane', almost exactly above the mO site. Even older resistivity (Radzilowski & Kummer, 1971) and Raman (Kaneda *et al.*, 1978) studies also suggested Li displacements either on or off the mirror plane by as much as ∼0.008 nm, and found additional support in another fairly old SC-XRef study carried out on a hydrated sample (Bates *et al.*, 1982). By contrast, a Rietveld full-profile refinement carried out on a polycrystalline Li-stabilized Na^+ β''-alumina, containing β-alumina in syntaxy, led Bera (1992) to conclude that Li^+ preferentially substitutes the octahedral Al(1) cations of the 'spinel block'. However, recent accurate refinements, converging to $R = 0.017$ for X-rays and $R = 0.036$ for neutrons and carried out at both low and room temperature, on a Li^+/Na^+ β-alumina, with Li making up 61% of the mobile cations (Edström, Gustafsson *et al.*, 1997), detected a totally different and far more complex structural situation. Li^+ is located in three distinct sites (Fig. 7): Li(1) is strictly on the 'conduction plane' together with all the residual non-exchanged Na^+, whereas Li(4) and Li(2) are outside that plane, being displaced by ∼0.05 and ∼0.10 nm, respectively, above and below, more or less on top of the site occupied by Li(1) and residual Na(1), which is in fact the BR site (compare Fig. 7 with Fig. 2). Moreover, the A site was found to be fully occupied by Na(3), thus leaving the aBR cation site empty and compelling all O(6) anions to move to the mO site in order to make the electrostatic charge distribution as even as possible. Edström, Gustafsson *et al.* (1997) appropriately stress the unique behaviour of Li^+ in the β-alumina host, but for the Al atom they state only that 'the structure comprises Al atoms octahedrally and tetrahedrally coordinated by O atoms to form spinel layers separated in the *c* direction by Al3—O5—Al3 bridging bonds'.

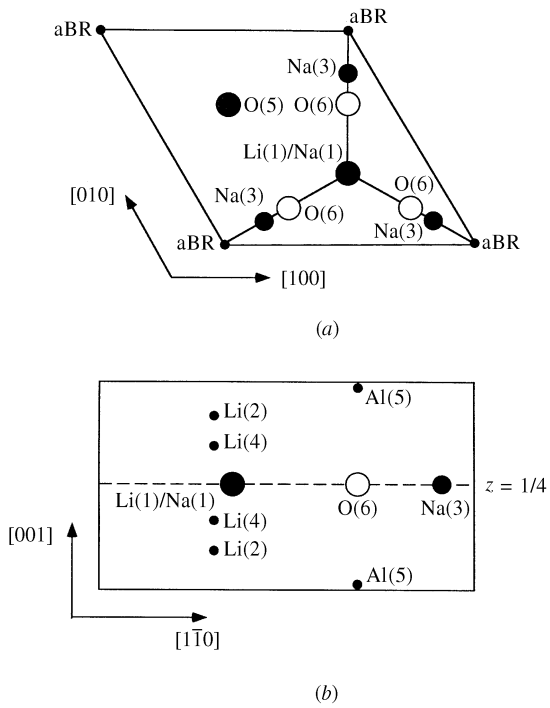

Figure 7
The structure of a 61% Li^+-exchanged Na^+ β-alumina, after Edström, Gustafsson *et al.* (1997; Figs. 3 and 4, considerably modified). (*a*) Projection of the 'conduction plane' on *ab* with the sites occupied by Li^+ and by the residual non-exchanged Na^+ and with two of the O anion sites. (*b*) Projection on the vertical plane intercepting the 'conduction plane' at $z = 1/4$, showing the out-of plane displacements of the Li(2) and Li(4) cations and the new position taken by O(6) from the previous mO site.

These crystal structure data (Edström, Gustafsson *et al.*, 1997) provide the clue needed to explain the unusual Al *K*-edge spectrum of Li^+ β-alumina. The Al atom that is situated on the *ab* plane bordering the 'spinel block' on both sides is Al(5), which is coordinated by four oxygens. Three of them, *i.e.*, two O(2) at 0.1776 nm and one O(4) at 0.1736 nm, are located inside the 'spinel block', whereas the fourth, O(6) at 0.1668 nm, is on the 'conduction plane' where it plays the role of bridging two opposite 'spinel blocks'. Because of the out-of-plane displacement of the Li(2) and Li(4) cations, the Al(5) at the interface, although not moving away from the 'spinel block', is now close enough to the fast-conducting cations (∼0.193 to ∼0.214 nm, respectively) to interact strongly with them. Actually, Al(5) is now close enough (∼0.227 nm) also to the site occupied by Li(1)/Na(1) to become able to interact with these two mobile cations too. Therefore, the enhanced heights of feature *A*, at least, and possibly also of feature *D*, result from these interactions, whereas all other features present over the *K* edge mostly arise from interactions between the O and Al atoms (both in four- and eightfold coordination, *e.g. C*) that are firmly located within the 'spinel block'.

5. Conclusions

In all β- and β''-alumina structures the Al^{3+} cations occupy sites that are essentially the same, irrespective of whether the 'spinel block' contains four layers or three, and of the hexagonal or trigonal overall symmetry of the compound. This is supported by the close similarity of the Al *K*-edge spectra recorded on all samples, and it can be detected through changes in the height of certain peaks. The only exception is Li^+-substituted β-alumina.

All β-aluminas show significant, and similar, degrees of Al structural disorder; better said, the long-range order distribution of Al is by far less regular in all of them (β- and β''-aluminas alike) than it is in α-alumina and in corundum (Mottana *et al.*, 1998). This statement holds true also for γ-alumina (Doyle *et al.*, 1999), and even for the Li^+ β-alumina, the uncommon Al *K*-edge spectrum of which, however, warrants deeper insight.

Compounds like β-aluminas, the structures of which consist of alternating layers of different composition with the Al cations in two different coordination modes, obviously have a lesser degree of long-range order than α-alumina, the structure of which is well known to consist of coordination arrays of identical edge-connected AlO_6 octahedra, lying flat on parallel planes, where the O anions are in a hexagonal closest packing arrangement (Newnham & deHaan, 1962). However, the broad IMS spectral features that indicate disorder over the long range for β- and β''-alumina alike do not contradict the evidence of short-range order around Al that is best deducible from FMS features.

In all β-alumina samples, the FMS features are similar with regard both to their shape and to their energy; Li^+-exchanged alumina is the only exception (see below). They can be assigned to fourfold- as well as sixfold-coordinated Al cations. However, each sample has characteristics of its own that seem to depend upon the atomic number of the fast-conducting cation located in its 'conduction plane'.

The Al local environments in the 'spinel block' are somewhat modified by interaction with the inter-block cations, when these have different electronic properties; these modifications mostly consist of changes in the height of certain absorption features, rather than the generation of new ones (for Li^+ β-alumina see below).

The broadness of all FMS features suggests that the disorder of the Al atoms in the 'spinel block' depends not only on the two different coordination motifs but also on the continuous range of minor variations exhibited in the Al—O bond distances.

A number of the local environments around Al that are present in β-aluminas are typical of octahedral Al as in α-alumina, *e.g.* those that give rise to its *A*, *B* and *C* spectral features; however, the very different intensities of these features reflect additional contributions arising from tetrahedral Al, as well as from the completely different multiple-scattering pathways.

In the absence of *ad hoc* multiple-scattering calculations, there is no simple explanation for the notably different Al *K*-edge spectrum exhibited by Li^+ β-alumina. Most likely, the Al *K*-edge spectrum of this compound reflects contributions from the interaction with three different kinds of Al ions. In addition to the contributions arising from the octahedral and tetrahedral Al ions inside the 'spinel block', strong effects originate from the fourfold-coordinated Al(5) ion located on the distal plane, *viz* proximal interfaces of the 'spinel block'; indeed, the small Li^+ ions displaced above and below the 'conduction plane' come so close to this Al(5) as to generate photo-electronic interactions that are not seen in any other β-alumina that contains bigger alkali cations.

This work was supported partly by a 1996 MURST grant to AM under project 'Aspetti cristallochimici cinetici e termodinamici' and partly by CNR grant CT97.00220.05 (together with A. Praturlon). Samples underwent ion exchange at the Department of Physics, Trento University, by Gino Mariotto, who generously made them available to us, together with the synthetic originals, through the interest of Francesco Rocca. The reference samples were provided by Fritz Seifert (Bayreuth). Experiments at the Al *K* edge (proposal No. 2317) were performed at SSRL, which is operated by Stanford University on behalf of the US Department of Energy, Office of Basic Energy Science. Thanks are due to Michael Rowen, Jeff Moore, Curtis Troxel, Paola de Cecco and the entire SSRL staff for assistance. At LNF, Antonio Grilli contributed with his technical skill. Critical reading by Francesco Rocca and by a unknown referee is gratefully acknowledged.

References

Alfrey, A. J., Stafsudd, O. M., Dunn, B. & Yang, D. L. (1988). *J. Chem. Phys.* **88**, 707–716.
Bates, J. B., Dudney, N. J., Brown, G. M., Wang, J. C. & Frech, R. (1982). *J. Chem. Phys.* **77**, 4838–4856.
Beevers, C. A. & Ross, M. A. S. (1937). *Z. Kristallogr.* **97**, 59–66.
Bera, J. (1992). *Solid State Commun.* **82**, 205–210.
Bettman, M. & Peters, C. R. (1969). *J. Phys. Chem.* **73**, 1174–1180.
Bianconi, A. (1988). *X-ray Absorption: Principles, Applications, Techniques of EXAFS, SEXAFS and XANES,* edited by D. C. Konigsberger & R. Prins, pp. 573–662. New York: Wiley.
Boilot, J.-P., Colomban, P., Collogues, R., Collin, G. & Comes, R. (1980). *J. Phys. Chem. Solids*, **41**, 253–258.
Bragg, W. L., Gottfried, C. & West, J. (1931). *Z. Kristallogr.* **77**, 255–274.
Briant, J. L. & Farrington, G. C. (1980). *J. Solid State Chem.* **33**, 385–390.
Briant, J. L. & Farrington, G. C. (1981). *J. Electrochem. Soc.* **128**, 1830–1834.
Bush, T. S., Catlow, C. R. A., Chadwick, A. V., Cole, M., Geatches, R. M., Greaves, G. N. & Tomlinson, S. M. (1992). *J. Mater. Chem.* **2**, 309–316.
Carrillo-Cabrera, W., Thomas, J. O. & Farrington, G. C. (1988). *Solid State Ionics*, **28–30**, 317–323.
Catti, M., Cazzanelli, E., Ivaldi, G. & Mariotto, G. (1987). *Phys. Rev. B*, **36**, 9451–9460.
Chaboy, J., Garcia, L. M., Bartolomé, F., Marcelli, A., Cibin, G., Maruyama, H., Pizzini, S., Rogalev, A., Goedkoop, J. B. & Goulon, J. (1998). *Phys. Rev. B*, **57**, 8424–8427.
Cheng, T. T., Aindow, M., Mayer, J. & Ruhle, M. (1994). *Philos. Mag. B*, **69**, 643–654.

Collin, G., Boilot, J.-P., Colomban, Ph. & Comes, R. (1986*a*). *Phys. Rev. B*, **34**, 5838–5849.
Collin, G., Boilot, J.-P., Colomban, Ph. & Comes, R. (1986*b*). *Phys. Rev. B*, **34**, 5850–5861.
Collin, G., Comes, R., Boilot, J. P. & Colomban, Ph. (1980). *Solid State Ionics*, **1**, 59–68.
Collin, G., Comes, R., Boilot, J.–P. & Colomban, Ph. (1988). *Solid State Ionics*, **28**–**30**, 324–332.
Dai, H. & Stafsudd, O. M. (1991). *J. Phys. Chem. Solids*, **52**, 367–379.
Den Boer, M. L., Pak, Y. S., Adamic, K. J., Greenbaum, S. G., Wintersgill, M. C., Lomax, J. F., Fontanella, J. J., Dunn, B. & Farrington, G. C. (1992). *Phys. Rev. B*, **45**, 6369–6375.
Doyle, C. S., Traina, S. J., Ruppert, H., Kandelewicz, T., Rehr, J. J. & Brown, G. E. Jr (1999). *J. Synchrotron Rad.* **6**, 621–623.
Dudney, N. J., Bates, J. B., Wang, J. C., Brown, G. M., Larson, B. C. & Engstrom, H. (1981). *Solid State Ionics*, **5**, 225–228.
Dunn, B., Farrington, G. C. & Thomas, J. O. (1989). *Mater. Res. Bull.* **14**, 22–30.
Dunn, B., Schwarz, B. B., Thomas, J. O. & Morgan, P. E. D. (1988). *Solid State Ionics*, **28**–**30**, 301–305.
Dunn, B., Yang, D. L. & Vivien, D. (1988). *J. Solid State Chem.* **73**, 235–242.
Edström, K., Gustafsson, T., Thomas, J. O. & Farrington, G. C. (1997). *Acta Cryst.* B**53**, 631–638.
Edström, K., Thomas, J. O. & Farrington, G. C. (1991*a*). *Acta Cryst.* B**47**, 210–216.
Edström, K., Thomas, J. O. & Farrington, G. C. (1991*b*). *Acta Cryst.* B**47**, 635–643.
Edström, K., Thomas, J. O. & Farrington, G. C. (1991*c*). *Acta Cryst.* B**47**, 643–650.
Edvardsson, S., Wolf, M. & Thomas, J. O. (1992). *Phys. Rev. B*, **45**, 10918–10923.
Erbil, A., Cargill, G. S., Frahm, R. & Boehme, R. F. (1988). *Phys. Rev. B*, **37**, 2450–2464.
Felsche, J. (1967). *Naturwissenschaften*, **54**, 612–613.
Fischer, P. (1967). *Z. Kristallogr.* **124**, 275–302.
Hussain, Z., Umbach, E., Shirley, D. A., Stohr, J. & Feldhaus, J. (1982). *Nucl. Instrum. Methods*, **195**, 115–131.
Jorgensen, J. D., Rotella, F. J. & Roth, W. L. (1981). *Solid State Ionics*, **5**, 143–146.
Kaneda, T., Bates, J. B. & Wang, J. C. (1978). *Solid State Commun.* **28**, 469–474.
Kato, K. (1968). *Disserationsarbeit*, Universität Hamburg.
Kummer, J. T. & Weber, N. (1968). *Trans. S. A. E.* **76**, 1003–1005.
Le Cars, Y., Comes, R., Deschamps, L. & Thery, J. (1974). *Acta Cryst.* A**30**, 305–309.
McKeown, G. A., Waychunas, G. A. & Brown, G. E. Jr (1985). *J. Non-Cryst. Solids*, **74**, 349–371.
Mariotto, G., Farrington, G. C. & Cazzanelli, E. (1985). *Transport–Structure Relations in Fast Ion and Mixed Conductors*, edited by F. W. Poulse, N. Hessel Andersen, S. Skaarup & O. T. Sorensen, pp. 455–460. Roskilde: Risø National Laboratory.
Mottana, A., Murata, T., Marcelli, A., Della Ventura, G., Cibin, G., Wu, Z. Y. & Tessadri, R. (1998). *J. Appl. Cryst.* **31**, 890–898.
Mottana, A., Robert, J.-L., Marcelli, A., Giuli, G., Della Ventura, G., Paris, E. & Wu, Z. Y. (1997). *Am. Mineral.* **82**, 497–502.
Natoli, C. R. & Benfatto, M. (1986). *J. Phys. C*, **8**, 11–23.
Newnham, R. E. & deHaan, Y. M. (1962). *Z. Kristallogr.* **117**, 235–237.
Peters, C. R., Bettman, M., Moore, J. W. & Glick, M. D. (1971). *Acta Cryst.* B**27**, 1826–1834.
Radzilowski, R. H. & Kummer, J. T. (1971). *J. Electrochem. Soc.* **118**, 714–716.
Rankin, G. A. & Merwin, H. E. (1916). *J. Am. Chem. Soc.* **38**, 568–586.
Reidinger, F. (1979). PhD thesis, State University of New York at Albany.
Rocca, F., Kuzmin, A., Purans, J. & Mariotto, G. (1994*a*). *Solid State Ionics*, **70**–**71**, 465–470.
Rocca, F., Kuzmin, A., Purans, J. & Mariotto, G. (1994*b*). *Phys. Rev. B*, **50**, 6662–6672.
Rocca, F., Kuzmin, A. & Purans, J. & Mariotto, G. (1996). *Phys. Rev. B*, **53**, 11444–11450.
Roth, W. L. (1972). *J. Solid State Chem.* **4**, 60–75.
Roth, W. L., Reidinger, F. & LaPlaca, S. (1976). *Superionic Conductors*, edited by G. D. Mahan & W. L. Roth, pp. 223–241. New York: Plenum Press.
Sattar, S., Ghosal, B., Underwood, M. L., Mertwoy, H., Saltzberg, M. A., Frydrych, W. S., Rohrer, G. S. & Farrington, G. C. (1986). *J. Solid State Chem.* **65**, 231–240.
Schaefers, F., Müller, B. R., Wong, J., Tanaka, T. & Kamimura, Y. (1992). *Synchr. Rad. News*, **5**(2), 28–30.
Thery, J. & Briançon, D. (1962). *C. R. Acad. Fr. Paris*, **254**, 2782–2785.
Tietz, F. & Urland, W. (1992). *J. Solid-State Chem.* **100**, 255–263.
Tofield, B. C. & Farrington, G. C. (1979). *Nature (London)*, **278**, 438–439.
Weber, N. & Venero, A. F. (1969). Technical Report No. SR69–102. Detroit: Ford Motor Co.
Wilkinson, A. P. (1997). *Inorg. Chem.* **36**, 1602–1607.
Wolf, M. & Thomas, J. O. (1993). *Acta Cryst.* B**49**, 491–496.
Wong, J., George, G. N., Pickering, I. J., Rek, Z. U., Rowen, M., Tanaka, T., Via, G. H., DeVries, B., Vaughan, D. E. W. & Brown, G. E. Jr. (1994). *Solid State Commun.* **91**, 559–561.
Wong, J., Shimkaveg, G., Goldstein, W., Eckart, M., Tanaka, T., Rek, Z. U. & Tompkins, H. (1990). *Nucl. Instrum. Methods Phys. Res. A*, **291**, 243–249.
Wong, R., Roth, W. L., Dunn, B. & Yang, D. L. (1986). *Solid State Ionics*, **18**–**19**, 599–602.
Wu, Z. Y., Marcelli, A., Mottana, A., Giuli, G., Paris, E. & Seifert, F. (1996). *Phys. Rev. B*, **54**, 2976–2979.
Yao, Y. F. & Kummer, J. T. (1967). *J. Inorg. Nucl. Chem.* **29**, 2453–2475.
Zendejas, M. & Thomas, J. O. (1990). *Phys. Scr. T*, **33**, 235–244.